PHYSICAL REVIEW A VOLUME 19, NUMBER 5 MAY 1979

L-subshell ionization cross sections for tungsten at low electron energies

Chu-Nan Chang*

Department of Physics, National Taiwan Normal University, Taipei, Taiwan, Republic of China and Department of Physics-Astronomy, California State University-Long Beach, Long Beach, California 90840

(Received 9 November 1978)

The L-subshell ionization cross sections for tungsten have been measured for incident electron beams of low energies. The electron energy was in the range of $1 < E/I_{L_i} \leq 4$. The values of the three L-subshell cross sections σ_{L_1}, σ_{L_2}, and σ_{L_3} were deduced from the thick-target yields of $L\beta_3$, $L\beta_1$, and $L\alpha_1$ x rays of tungsten. A differential method was employed in the deduction procedures. The x-ray spectra were obtained by an improved version of a single-crystal, high-angle goniometer. The shape of the energy dependence of the measured cross sections deviates from the predictions given by McGuire's scaling result as well as Gryzinski's classical scaling result.

I. INTRODUCTION

The plane-wave Born approximation (PWBA) and other approximations predict, in the nonrelativistic limit, a scaling law for the K-shell ionization cross sections for all target elements under bombardments by electrons[1] and fast light ions.[2] The product of the cross section σ_{1s} and the square of the $1s$-shell ionization energy is a universal function of the projectile energy in units of $1s$-shell ionization energy, i.e., $\sigma_{1s}(I_{1s})^2 = f(E/\lambda I_{1s})$, where λ is the mass ratio of the incident particle to the electron. This scaling is an essential feature of the Coulomb excitation of an atom by the bombardments of charged particles.

The existing data for K-shell ionization cross sections indicates this general gross feature, even though the scaling overestimates the ionization cross section at low bombarding energies. Recently, scaled electron ionization cross sections of atomic subshells (other than the K shell) in the Born approximation were obtained by McGuire.[3] This scaling has, in general, a nonclassical feature, i.e., it does not vary inversely with the square of the ionization energy. Thus cross section measurements for the electron ionization of atomic subshells are important in assuring the applicability of this scaling law in various energy regions.

There are a few experimental data on the cross sections of electron ionization of atomic L subshells,[4] and they do not quite agree with each other, especially at low electron energies. I report here measurements of the total L-subshell ionization cross sections of tungsten under electron bombardment at low energy E, in the range $1 < E/I_{L_i} \leq 4$, where I_{L_i} is the ionization energy of the ith L subshell ($i = 1, 2, 3$). The three L-subshell ionization cross sections of tungsten, σ_{L_1}, σ_{L_2}, and σ_{L_3}, were deduced from the thick-target yields of $L\beta_3$, $L\beta_1$ and $L\alpha_1$ x rays of tungsten. A differential method was employed in the deduction procedures. The x-ray spectra were obtained by an improved version of a single-crystal, high-angle goniometer.

The shape of the energy dependence of the measured cross sections deviates from the predictions of McGuire's nonclassical scaling result[3] as well as from Gryzinski's classical scaling result.[5] In the very-low-energy region ($E/I_{L_i} < 1.5$) the measured cross sections fall off less than those predicted by these two scalings.

II. EXPERIMENT

A thick block of tungsten, 99.9% pure, was bombarded by an electron beam of known energy and flux. The electron beam was generated by a homemade electron gun in which the tungsten filament was fitted in a stainless-steel focusing cup. An insulated transformer supplied the filament with the heating current. A high-voltage power supply connected in series with a voltage regulator and a ripple suppressor and rated at less than 0.3% ripple at a full load of 120 kV and 30 mA was used to accelerate the electron beam. For our present work, the load was kept at a constant current of 0.3 mA and a voltage of 12–40 kV. The target was tilted such that the normal of the target surface was 7.73° from the incident-beam direction. This arrangement makes the takeoff angle θ of the emitting characteristic x ray of the target 7.73°. These x rays pass through a thin (0.254-mm) beryllium window which was lined up with the entrance Soller slits of the single-crystal goniometer. The wavelength of the x ray was analyzed by a calcite single crystal and the diffracted x ray was detected by a NaI(Tl) detector with a 0.127-mm beryllium window.

The x-ray spectra of $L\beta_3$, $L\beta_1$, and $L\alpha_1$ were

taken by scanning the target x rays in steps. Each step consisted of a change of $2\theta = 0.01°$ and a one-min interval. The tungsten x ray spectra of $L\beta_3$, $L\beta_1$ and $L\alpha_1$ at an electron energy of 20 keV are shown in Fig. 1. The full width of the half maximum of the $L\alpha_1$ x ray was measured to be 18 eV. This high-resolution spectrum has the advantage of eliminating the contamination, if any, present in the target. The $L\beta_3$ and $L\beta_1$ x rays can be resolved well, and so the cross sections σ_{L_1} and σ_{L_2} can be readily deduced. However, the efficiency of the single-crystal goniometer is very small (on the order of 10^{-7}), so at low electron energy a reasonably good yield can be obtained only by using a thick target without too much of a change of beam current. This is especially true for $L\beta_3$ x rays.

III. DATA ANALYSIS AND RESULTS

The x-ray production cross section at an incident energy can be obtained by differentiating the measured x-ray yields of the thick target, $Y_{L_x}(E)$ [here $Y_{L_x}(E)$ has already been corrected for the electron rediffusion effect[6]];

$$\sigma_{L_x}(E) = \frac{f}{In\epsilon_x} \frac{Y_{L_x}(E) - FY_{L_x}(E-\Delta E)}{\Delta R}$$

$$= \frac{f}{In\epsilon_x}\left(\frac{Y_{L_x}(E) - Y_{L_x}(E-\Delta E)}{\Delta E}\frac{\Delta E}{\Delta R} + (1-F)Y_{L_x}(E-\Delta E)\frac{1}{\Delta R}\right), \quad (1)$$

where the terms have the following definitions: I is the total number of the incident electron, and is 1.124×10^{14} for 0.3 mA min in the present work. n is the number of atoms per unit volume of the target material. For tungsten, $n = 3.121\times10^{22}$/g. ϵ_x is the detection efficiency of the goniometer, including the reflectivity of the calcite crystal, the counting efficiency of the NaI(Tl) detector, the solid-angle correction, and the attenuation of the photon path through the beryllium windows and air. f is the fraction of direct ionization by electron bombardments. This quantity was found to be about 67% and independent of the electron energy.[7] F is a correction factor for the intensity of the x rays emitted from a layer of thickness ΔR. For a takeoff angle of θ,

$$F = e^{-\Delta R\mu\csc\theta},$$

where μ is the mass-absorption coefficient of the target material for the analyzed x rays.

As $\Delta R \to 0$ and $\Delta E \to 0$, Eq. (1) becomes

$$\sigma_{L_x}(E) = \frac{f}{In\epsilon_x}\left(\frac{dY_{L_x}(E)}{dE}\frac{dE}{dR} + \mu\csc\theta Y_{L_x}(E)\right), \quad (2)$$

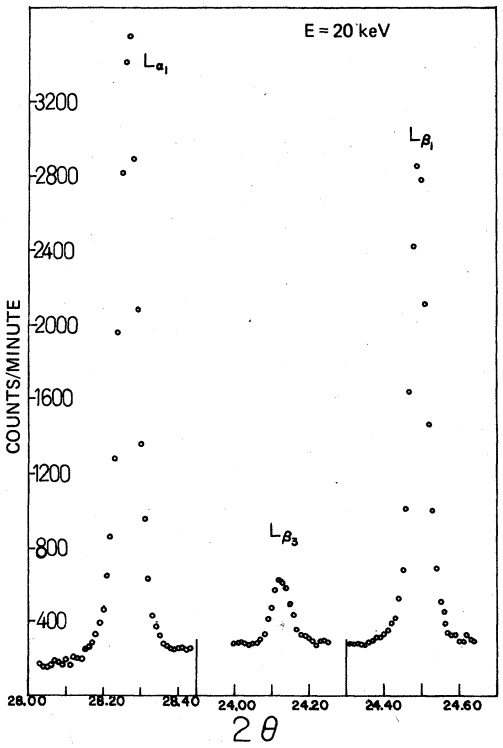

FIG. 1. $L\beta_3$, $L\beta_1$, and $L\alpha_1$ x rays of a thick-tungsten target at electron energy of 20 keV. The spectra were obtained from an improved high-angle, single-crystal goniometer.

where $dY_{L_x}(E)/dE$ is the slope of the excitation function of the measured x-ray yields and dE/dR is the stopping power of tungsten for electrons. Note that all subscripts x in Eqs. (1) and (2) represent a particular L-x-ray line, such as $L\beta_3$, $L\beta_1$, or $L\alpha_1$. For example, $\sigma_{L\alpha_1}$ represents the x-ray production cross section of the $L\alpha_1$ line.

To evaluate dE/dR, one may have to take the contribution of bremsstrahlung[8] into account. In the energy region under consideration, however, this contribution is three orders of magnitude smaller than that due to collision and can therefore be neglected. Bethe's nonrelativistic formula[9] was used to calculate dE/dR for tungsten. Numerically, it was found to be

$$dE/dR = 31\,460\ln(1.7059E)/E \text{ keV cm}^2/\text{g}. \quad (3)$$

The relativistic correction for dE/dR was found to be negligible at $E = 40$ keV ($v/c = 0.374$).

The excitation function of the thick-target yields of L x rays could follow the empirical law[10] $Y_{L_x}(E) = K(E/I_{L_i}-1)^n$, where K and n are adjustable parameters. Measured yields of $L\beta_3$, $L\beta_1$, and $L\alpha_1$ x rays were plotted versus $(E/I_{L_i}-1)$ on a full-log scale in Fig. 2. These are not quite straight lines because I did not correct for the target self-absorption effect. I then deduced the slope

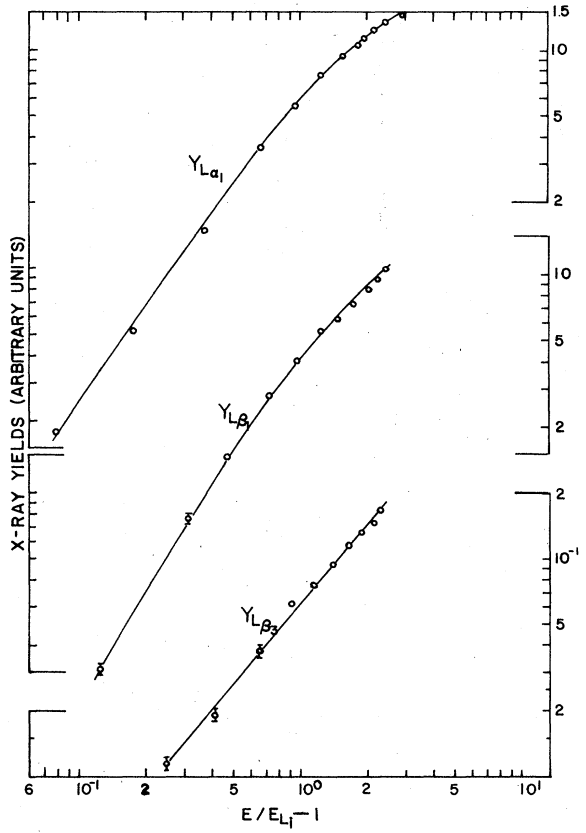

FIG. 2. $L\beta_3$, $L\beta_1$, and $L\alpha_1$, x-ray production yields plotted vs $E/I_{L_i}-1$ on a full-log scale. The x-ray production yields have been corrected for the effect of electron rediffusion.

$dY_{L_x}(E)/dE$ by fitting the measured x-ray yields $Y_{L_x}(E)$ to a polynomial function of E. The experimental and fitted values of $Y_{L_x}(E)$ and the slopes $dY_{L_x}(E)/dE$ are listed in Tables I(a)–I(c).

The x-ray production cross section $\sigma_{L_x}(E)$ for $L\beta_3$, $L\beta_1$, and $L\alpha_1$ x rays can readily be deduced from Eq. (2), provided that f/ϵ_x is known. Since f is independent of energy, it can be absorbed into ϵ_x and make $f/\epsilon_x = 1/\epsilon_x'$. The $\epsilon'_{L\beta_3}$, $\epsilon'_{L\beta_1}$, and $\epsilon'_{L\alpha_1}$ can only differ from each other through their different photon-absorption coefficients in air and beryllium windows. Here the photon path through air (=38.5 cm) and the total thickness of the beryllium windows (=0.38 mm) make $\epsilon'_{L\beta_1}/\epsilon'_{L\beta_3} = 0.952$, $\epsilon'_{L\alpha_1}/\epsilon'_{L\beta_3} = 0.833$, and $\epsilon'_{L\alpha_1}/\epsilon'_{L\beta_1} = 0.875$.[11] The relative total ionization cross sections for each L subshell, $\epsilon'_{L\beta_3}\sigma_{L_1}$, $\epsilon'_{L\beta_1}\sigma_{L_2}$, and $\epsilon'_{L\alpha_1}\sigma_{L_3}$ can be obtained through the following formulas:

$$\epsilon'_{L\beta_3}\sigma_{L\beta_3} = \epsilon'_{L\beta_3}\sigma_{L_1}\omega_1 F_{1\beta_3}, \tag{4a}$$

$$\epsilon'_{L\beta_1}\sigma_{L\beta_1} = (\epsilon'_{L\beta_1}\sigma_{L_2} + \epsilon'_{L\beta_1}/\epsilon'_{L\beta_3}\epsilon'_{L\beta_3}\sigma_{L_1} f_{12})\omega_2 F_{2\beta_1}, \tag{4b}$$

$$\epsilon'_{L\alpha_1}\sigma_{L\alpha_1} = (\epsilon'_{L\alpha_1}\sigma_{L_3} + \epsilon'_{L\alpha_1}/\epsilon'_{L\beta_1}\epsilon'_{L\beta_1}\sigma_{L_2} f_{23} + \epsilon'_{L\alpha_1}/\epsilon'_{L\beta_3}\epsilon'_{L\beta_3}\sigma_{L_1} f_{13})\omega_3 F_{3\alpha_1}, \tag{4c}$$

where ω_1, ω_2, and ω_3 are the L-subshell fluorescence yields, f_{12}, f_{23}, and f_{13} are the Kronig transition probabilities,[12] and $F_{3\alpha_1}$, $F_{2\beta_1}$, and $F_{1\beta_3}$ are the fractional widths for the $L\alpha_1$, $L\beta_1$, and $L\beta_3$ x rays, respectively.[13] These relative ionization cross sections were then scaled to the values of σ_{L_1}, σ_{L_2}, and σ_{L_3} calculated according to the McGuire scaling at $E = 40$ keV. The respective values of $\epsilon'_{L\beta_3}$, $\epsilon'_{L\beta_1}$, and $\epsilon'_{L\alpha_1}$ were then found to be 5.33×10^{-7}, 4.58×10^{-7}, and 3.98×10^{-7}. Using these values, I obtained a new set of ratios, $\epsilon'_{L\beta_1}/\epsilon'_{L\beta_3} = 0.859$, $\epsilon'_{L\alpha_1}/\epsilon'_{L\beta_3} = 0.747$, and $\epsilon'_{L\alpha_1}/\epsilon'_{L\beta_1} = 0.870$. The first two are about 12% smaller than those calculated above (by considering the different absorption coefficients in air and mylar for the different x-ray lines of $L\beta_3$, $L\beta_1$, and $L\alpha_1$), while the third is comparable to that calculated above. It is therefore reasonable to assume that the value of $\epsilon'_{L\beta_3}$ is scaled too high. Furthermore, the previously calculated value $\epsilon'_{L\beta_1}/\epsilon'_{L\beta_3} = 0.952$ must be considered more suitable, since the energies of the $L\beta_3$ and $L\beta_1$ x rays are very close to each other and this ratio should thus be close to unity. Accordingly, we take the following set of values to be the "effective efficiency" of the detecting system: $\epsilon'_{L\beta_3} = 4.7\times10^{-7}$, $\epsilon'_{L\beta_1} = 4.5\times10^{-7}$, ans $\epsilon'_{L\alpha_1} = 3.9\times10^{-7}$. These values can be considered accurate to within 5%. If these values are wrong, multiplication by a constant factor should correct them.

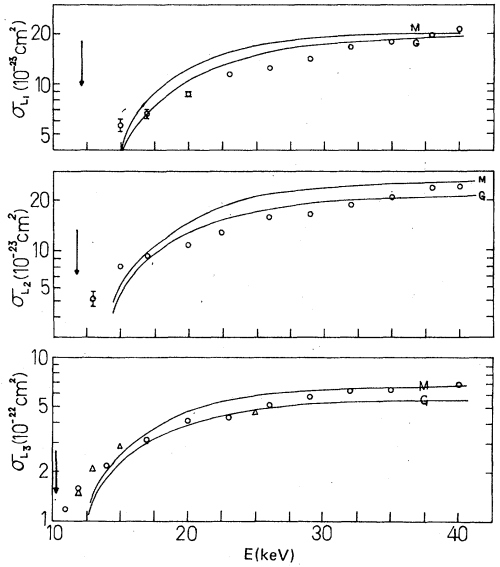

FIG. 3. Individual L-subshell ionization cross sections. The two solid curves represent the results scaled with the McGuire scaling (M) and the Gryzinski scaling (G). Circles represent the measurements for $\theta = 7.73°$, and triangles the measurements for $\theta = 3.3°$. The three vertical arrows indicate the threshold of the three subshells of L_1, L_2, and L_3.

TABLE I. (a) Tungsten L_1-subshell ionization cross sections $\sigma_{L_1}(E)$ for incident electrons of energy E. Column 2 is the measured thick-target yields of $L\beta_3$ x-rays, $Y_{L\beta_3}(E)$ and the fitted yields $Y^f_{L\beta_3}(E)$ in units of x rays per incident particle. Column 3 is the slope of the excitation function. Column 4 is the relative $L\beta_3$ x-ray production cross sections in cm^2. Column 5 is the L-subshell ionization cross sections in cm^2, as determined by Eq. (4) with $\epsilon'_{L\beta_3}=4.7\times10^{-7}$. (b) Tungsten L_2-subshell ionization cross sections $\sigma_{L_2}(E)$ for incident electrons of energy E. The rest of the description is the same as in (a), except that $L\beta_3$ is changed to $L\beta_1$ and $\epsilon'_{L\beta_1}=4.5\times10^{-7}$. (c) Tungsten L_3-subshell ionization cross sections $\sigma_{L_3}(E)$ for incident electrons of energy E. The rest of the description is same as in (a) except that $L\beta_3$ is changed to $L\alpha_1$ and $\epsilon'_{L\alpha_1}=3.9\times10^{-7}$. The negative numbers represent negative powers of ten, for example, $1.14-11=1.14\times10^{-11}$.

	E (keV)	$Y_{L\beta_3}(E)$ (x rays/particle ±3%)	$Y^f_{L\beta_3}(E)$	$dY^f_{L\beta_3}(E)/dE$ (x rays/keV particle ±10%)	$\epsilon'_{L\beta_3}\sigma_{L\beta_3}$ (cm^2 ±12%)	$\sigma_{L_1}(E)$ (cm^2 ±17%)
	15	1.14 −11	1.14 −11	4.49 −12	1.25 −30	5.64 −23
	17	1.89 −11	1.91 −11	5.23 −12	1.45 −30	6.56 −23
	20	3.76 −11	3.98 −11	5.64 −12	1.93 −30	8.68 −23
	23	6.31 −11	5.71 −11	5.87 −12	2.50 −30	1.13 −22
(a)	26	7.48 −11	7.50 −11	6.04 −12	2.73 −30	1.23 −22
	29	9.20 −11	9.33 −11	6.18 −12	3.10 −30	1.40 −22
	32	1.17 −10	1.12 −10	6.31 −12	3.66 −30	1.65 −22
	35	1.29 −10	1.31 −10	6.41 −12	3.93 −30	1.77 −22
	38	1.44 −10	1.51 −10	6.51 −12	4.26 −30	1.92 −22
	40	1.64 −10	1.64 −10	6.57 −12	4.73 −30	2.14 −22
	E (keV)	$Y_{L\beta_1}(E)$ (x rays/particle ±1%)	$Y^f_{L\beta_1}(E)$	$dY^f_{L\beta_1}(E)/dE$ (x rays/keV particle ±10%)	$\epsilon'_{L\beta_1}\sigma_{L\beta_1}$ (cm^2 ±10%)	$\sigma_{L_2}(E)$ (cm^2 ±15%)
	13	1.55 −11	1.43 −11	2.07 −11	5.37 −30	5.08 −23
	15	7.50 −11	8.09 −11	3.45 −11	9.42 −30	8.00 −23
	17	1.45 −10	1.56 −10	3.50 −11	1.07 −29	9.24 −23
	20	2.76 −10	2.91 −10	3.55 −11	1.34 −29	1.08 −22
	23	4.01 −10	3.97 −10	3.59 −11	1.61 −29	1.28 −22
(b)	26	5.46 −10	5.06 −10	3.62 −11	1.94 −29	1.57 −22
	29	6.12 −10	6.15 −10	3.65 −11	2.07 −29	1.65 −22
	32	7.28 −10	7.26 −10	3.67 −11	2.34 −29	1.86 −22
	35	8.46 −10	8.35 −10	3.68 −11	2.62 −29	2.09 −22
	38	9.68 −10	9.46 −10	3.70 −11	2.91 −29	2.36 −22
	40	1.02 − 9	1.02 − 9	3.71 −11	3.03 −29	2.43 −22
	E (keV)	$Y_{L\alpha_1}(E)$ (x rays/particle ±0.6%)	$Y^f_{L\alpha_1}(E)$	$dY_{L\alpha_1}(E)/dE$ (x rays/keV particle ±10%)	$\epsilon'_{L\alpha_1}\sigma_{L\alpha_1}$ (cm^2 ±10%)	$\sigma_{L_3}(E)$ (cm^2 ±15%)
	11	1.79 −11	1.74 −11	3.02 −11	8.78 −30	1.17 −22
	12	5.08 −11	5.36 −11	4.14 −11	1.24 −29	1.54 −22
	14	1.50 −10	1.51 −11	5.52 −11	1.81 −29	2.23 −22
	17	3.57 −10	3.39 −10	6.91 −11	2.69 −29	3.17 −22
(c)	20	5.51 −10	5.63 −10	7.96 −11	3.43 −29	4.09 −22
	23	7.56 −10	7.56 −10	5.63 −11	3.67 −29	4.30 −22
	26	9.35 −10	9.35 −10	5.57 −11	4.24 −29	5.01 −22
	29	1.06 − 9	1.07 − 9	6.92 −11	4.83 −29	5.73 −22
	32	1.22 − 9	1.18 − 9	6.90 −11	5.33 −29	6.26 −22
	35	1.31 − 9	1.29 − 9	6.90 −11	5.43 −29	6.34 −22
	40	1.46 − 9	1.45 − 9	6.87 −11	6.06 −29	6.89 −22

The three L-subshell total cross sections were then obtained from Eqs. (2) and (4) and tabulated in Tables I(a)–I(c). These were also plotted in Fig. 3.

The error bars in Fig. 3 are purely statistical. The main uncertainties in the measured values of σ_{L_1}, σ_{L_2}, and σ_{L_3} were due to the uncertainties of the atomic parameters (5%), the deduced slope $dY_{L_x}(E)/dE$ (10%), and the stopping power dE/dR (10%). There is no interference from K ionization, since the K-ionization threshold energy of tungsten (69.5 keV) is higher than the highest bombarding energy (40 keV) used in the measurements.

In order to check the validity of my data-deduction procedures, additional measurements were made at $\theta=3.3^0$ for the $L\alpha_1$ x rays. The deduced total ionization cross sections of σ_{L_3} were also plotted in Fig. 3. The total uncertainty of my relative cross sections was estimated to be about 15%.

IV. DISCUSSION

The classical scaling law predicted by Gryzinski can be written

$$\sigma_{L_i} = b_{L_i} \frac{\sigma_0}{I_{L_i}} \frac{1}{x} \left(\frac{x-1}{x+1} \right)^{3/2} \times \left[1 + \frac{2}{3} \left(1 - \frac{1}{2x} \right) \ln[2.7 + (x-1)^{1/2}] \right],$$

where b_{L_i} is the number of electrons on the subshell L_i, $x = E/I_{L_i}$, and $\sigma_0 = 6.56 \times 10^{-14}$ cm^2 eV^2. This formula can be rewritten

$$I_{L_i}^2 \sigma_{L_i} = b_{L_i} f(E/I_{L_i}) .$$

This classical scaling apparently predicts the same value of $f(E/I_{L_i})$ at the same value of E/I_{L_i} for all subshells. While McGuire's nonclassical scaling predicts this same feature of $f(E/I_{L_i})$ only for the subshells having the same orbital angular momentum, such as $2p_{1/2}$ and $2p_{3/2}$. Thus the shapes of these two predicted ionization cross sections of the L_1 subshell ($2s_{1/2}$), σ_{L_1}, are different from each other as expected (see Fig. 3).

The L-subshell ionization cross sections calculated from Gryzinski's classical scaling were plotted in Fig. 3 and were denoted by G, and those calculated from McGuire's nonclassical scaling were also plotted in the same figure and denoted by M. McGuire's predictions were 5% – 20% higher than those of Gryzinski. The shape of the energy dependence of my measured cross sections follows neither of these predictions. Substantial discrepancies between my measurements and the two theories were observed at energies below about 20 keV.

In order to compare my measured cross sections to the other existing data for different elements, the universal functions $f(E/I_{L_i})$ was used. In a comparison of my measurements of σ_{L_3} for tungsten with the measurements of $\sigma_{L_{2,3}}$ for Ar by Langenberg *et al.*[4] and the measurements of σ_{L_3} for Au by Davis *et al.*,[4] the $\sigma_{L_{2,3}}$ of Ar and σ_{L_3} for Au were normalized to McGuire's scaled values at $E/I_{L_3} = 4.0$ and 5.0, respectively. The universal functions $f(E/I_{L_3})$ of Ar, W, and Au were plotted with the scaled values (the solid curve) in Fig. 4. My data agree with those of Langenberg *et al.* Nevertheless, the measured values tend to fall off less rapidly than the scaled values at very low electron energies. This disagreement is expected since the Born approximation is not expected to be accurate near the threshold energy. But one should note that the Born approximation usually predicts higher cross sections at low energies. This is in contradiction to what I have observed.

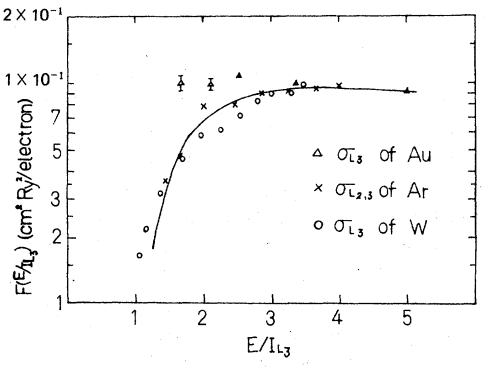

FIG. 4. Comparison of my measured cross sections σ_{L_3} of W to the cross sections of Ar and Au (Ref. 4) through the universal function $f(E/I_{L_3})$. The cross sections of Ar and Au were normalized to McGuire's scaled values at $E/I_{L_3} = 4$ and 5, respectively.

My measured cross sections may have been scaled (through the values of $\epsilon'_{L\beta_3}$, $\epsilon'_{L\beta_1}$, and $\epsilon'_{L\alpha_1}$) too high. The absolute cross sections of Ar measured by Langenberg *et al.* were found to agree with those calculated according to the McGuire scaling quite well at $E/I_{L_3} \geq 10$, while below this energy they are lower than the calculated values. The agreement at high energy is a reasonable result so far as Born approximation is concerned. However, even if we normalize my measured cross sections to those of Ar at $E/I_{L_3} = 4.0$, the two lowest-energy data of σ_{L_3} for tungsten are still substantially higher than those predicted by McGuire's scaling.

In a thick solid target, there is the effect of multiple scattering. Due to the complexity of this effect, I have not included it in the data-deduction procedure. Nevertheless, the scattering effect was found to be discernible, even with a thin solid target, in the light-ion–atom collision for low bombarding energies.[14] So the effect of multiple scattering may affect the shape of the energy dependence of the measured ionization cross sections.

Since the thick-target yields should be reduced by the correction for the multiple scattering of the incident electron in the thick target, the correction factor, $f_M(E)$ for $Y_{L_x}(E)$ in Eqs. (1) and (2) has values between 0 and 1. The range of the incident electron in the target is also affected by multiple scattering, and the effect is stronger for incident electrons of lower energy. So the correction factor $f_M^{\Delta R}$ is greater than 1 for ΔR in Eq. (1). For simplicity, we assume that $f_M(E) = f_M(E - \Delta E)$. Then Eq. (2) should be corrected by multiplying its first term by a factor $f_M(E)/f_M^{\Delta R}$ and its second term by a factor $f_M(E)$.

In the data-deduction procedure I found that the

first term of Eq. (2) dominates the x-ray production cross sections when the bombarding energies of the incident electrons is below about 20 keV, and that the second term of Eq. (2) becomes dominant when the bombarding energy is above about 30 keV. So the shape of the energy dependence of the measured cross sections should be altered by the effect of the multiple scattering, and the low-energy portion of the data may fall off more rapidly than shown in Fig. 3, as $f_M(E)/f_M^{\Delta R}$ and $f_M(E)$ may fall off with the energy. Thus the discrepancies between the data and the predictions of the scalings may be partially due to the effect of multiple scattering. But one should also note that the factor $f_M(E)$ should be a slowly varying function of energy, since this factor is proportional to the product of two quantities; one relates to the degree of multiple scattering and the other relates to the probability of producing x rays. The good agreement of our tungsten data with the argon data of Langensberg *et al.* (see Fig. 4) indicates that the correction factor $f_M(E)$ is nearly a flat function of energy in the energy range $1.5 \lesssim E/I \lesssim 4$. Therefore the large discrepancies observed near the threshold may not be completely corrected by the effect of multiple scattering. However, further experimental study is needed to clarify this point.

V. CONCLUSION

The differential method used to analyze the thick-target x-ray yields in order to obtain inner-shell ionization cross sections provides a way to measure the cross sections down to the electron energy $E/I \simeq 1$. For L-subshell ionization cross sections, the maximum occurring at $E/I \simeq 3.5$ is in agreement with the predictions of either the classical theory of Gryzinski or the nonclassical scaling law of McGuire (see Fig. 4). But the observed cross sections fall off less than these two predictions at very low energies.

The pronounced difference between the shapes of the energy dependence of the cross sections of the three L subshells of tungsten obtained experimentally in comparison to the scaled values indicates that more investigation is needed both experimentally and theoretically for heavy elements at low electron energies for a better understanding of the inner-shell ionization processes for the heavy elements.

ACKNOWLEDGMENTS

The author wishes to thank Professor S. I. Salem for his help with the instrument and for some useful discussions. This work was supported in part by the NSC of the Republic of China.

---

*Permanent address: Department of Physics, National Taiwan Normal University, Taipei, Taiwan, Rep. of China.

[1]C. J. Powell, Rev. Mod. Phys. 48, 33 (1976).
[2]J. D. Garcia, R. J. Fortner, and T. M. Kavanagh, Rev. Mod. Phys. 45, 111 (1973).
[3]E. J. McGuire, Phys. Rev. A 16, 73 (1977).
[4]D. V. Davis, V. D. Mistry, and C. A. Quarles, Phys. Lett. A 38, 169 (1972); A. Langenberg, F. J. de Heer, and J. Van Eck, J. Phys. B 8, 2079 (1975); S. I. Salem, and L. D. Moreland, Phys. Lett. A 37, 161 (1971).
[5]M. Gryzinski, Phys. Rev. 138, A336 (1965).
[6]D. L. Webster, W. W. Hansen, and F. B. Duveneck, Phys. Rev. 44, 258 (1933).
[7]S. I. Salem and D. G. Zarlingo, Phys. Rev. 155, 7 (1967).
[8]G. Knop and W. Paul, in *Alpha-, Beta-, and Gamma-Ray Spectroscopy*, edited by Siegbahn (American Elsevier, New York, 1968), Vol. 1, p. 15.
[9]H. A. Bethe, Ann. Phys. (Leipzig) 5, 325 (1930); in *Alpha-, Beta-, and Gamma-Ray Spectroscopy*, edited by K. Siegbahn (American Elsevier, New York, 1968), Vol. 1, p. 12.
[10]See Ref. 6 and references cited therein.
[11]Evaluated from the photon cross sections of E. Storm and H. I. Israel, Nucl. Data Table A 7, 565 (1970).
[12]W. Bambynek *et al.*, Rev. Mod. Phys. 44, 716 (1972).
[13]J. H. Scofield, Phys. Rev. 179, 9 (1969).
[14]G. Basbas, W. Brandt, and R. Laubert, Phys. Rev. A 17, 1655 (1978).